



Experimental study on the membrane distillation of highly mineralized mine water

Ji Qi¹ · Jiafeng Lv¹ · Wei Bian² · Jingfeng Li² · Shuqin Liu¹

Received: 26 August 2020/Revised: 20 October 2020/Accepted: 22 April 2021/Published online: 14 July 2021
© The Author(s) 2021

Abstract Membrane distillation (MD) is a promising membrane separation technique used to treat industrial wastewater. When coupled with cheap heat sources, MD has significant economic advantages. Therefore, MD can be combined with solar energy to realize the large-scale and low-cost treatment of highly mineralized mine water in the western coal-producing region of China. In this study, highly mineralized mine water from the Ningdong area of China was subjected to vacuum MD (VMD) using polyvinylidene fluoride hollow-fiber membranes. The optimal operation parameters of VMD were determined by response surface optimization. Subsequently, the feasibility of VMD for treating highly mineralized mine water was explored. The fouling behavior observed during VMD was further investigated by scanning electron microscopy with energy-dispersive X-ray spectroscopy (SEM–EDS). Under the optimal parameters (pressure = -0.08 MPa, temperature = 70 °C, and feed flow rate = 1.5 L/min), the maximum membrane flux was 8.85 kg/(m^2 h), and the desalination rate was 99.7% . Membrane fouling could be divided into three stages: membrane wetting, crystallization, and fouling layer formation. Physical cleaning restored the flux and salt rejection rate to 94% and 97% of the initial values, respectively; however, the cleaning interval and cleaning efficiency decreased as the VMD run time increased. SEM–EDS analysis revealed that the reduction in flux was caused by the precipitation of $CaCO_3$. The findings also demonstrated that the membrane wetting could be attributed to the formation of NaCl on the cross section and outer surface of the membrane. Overall, the results confirm the feasibility of MD for treating mine water and provide meaningful guidance for the industrial application of MD.

Keywords Mine water · Membrane distillation · Operating parameters · Membrane fouling

1 Introduction

The western region of China, which is the nation's main coal-producing region, accounts for 77% of national coal output (Dazhao et al. 2016; Limin et al. 2019). However, water scarcity in the region accounts for only 7.9% of the

national total (China Water Resources Bulletin 2018). The production of mine water must be accompanied by coal mine exploitation. According to statistical data, the utilization rate of mine water in China is less than 30% (Binbin et al. 2018). The major reason for this phenomenon is that the salt content of mine water from the western region of China is high compared to mine waters from other regions; the proportion of mine water with high salinity in the northwest region exceeds 50% (Fuqin et al. 2018). The direct discharge of highly mineralized mine water will cause ecological damage, soil salinization, and waste. Therefore, low-cost treatment strategies for high-salinity mine water are urgently needed.

Traditional thermal desalination requires a large amount of heat energy. Comparatively, the reverse osmosis

✉ Shuqin Liu
liushuqin@cumtb.edu.cn

¹ School of Chemical and Environmental Engineering, China University of Mining and Technology, Beijing 100083, China

² State Key Laboratory of Water Resource Protection and Utilization in Coal Mining, China Energy Investment Corporation, Beijing 100011, China

treatment of mine water has several advantages in terms of wastewater quality, power consumption, desalination efficiency, and land use. However, the current state has put forward higher requirements for mine water treatment. New coal mines in some areas are required to achieve zero liquid discharge (Dazhao et al. 2016). Hence, as an emerging desalination technique, membrane distillation (MD) has attracted increasing attention due to its competitive features (Alkudhri et al. 2012; Drioli et al. 2015; Sun et al. 2014). Compared to other processes, MD has lower heat requirements. Elena et al. (2014) combined solar heat with MD and conducted a long-term pilot study. Guillen et al. (2013) used seawater for a series of dry/wet cycles to simulate intermittent MD operation, which proved that hydrophobic membrane has chemical stability and anti-drying performance in MD operation, and could reduce the wetting phenomenon of membrane.

Based on the author's previous studies on early-stage MD, many industries (e.g., pit power plants and coal chemical plants) that generate substantial industrial waste heat are located near the western mining area. Figure 1 shows a diagram of a solar photothermal VMD system. In this system, highly mineralized mine water is heated in the solar collectors. After reaching a predetermined temperature, the mine water enters the hot side of the membrane assembly under the action of the peristaltic pump. The hydrothermal fluid is then subjected to VMD under the action of the temperature difference.

The availability of a cheap heat source is the economic basis for the large-scale application of MD. Wei et al. (2020) compared the equipment requirements and energy consumption of MD based on various cheap heat sources.

MD has some of the same problems as other membrane-based technologies such as forward osmosis and nanofiltration. For example, the fouling and wetting of the hydrophobic membrane cause the permeate flux to decrease, resulting in the deterioration of permeate quality (Guillen-Burrieza et al. 2013). Julian et al. (2018) evaluated the kinetics of calcium carbonate (CaCO_3) fouling

during MD based on numerical modeling and found that the temperature and concentration polarization have significant effects on the CaCO_3 deposition rate. Laqbaqbi et al. (2018) used direct contact MD to treat textile wastewater, explored the fouling phenomenon on the membrane surface and pores using various characterization techniques, and determined the irreversible fouling index and flux reduction factor.

The objectives of the present study were to: (1) use MD to treat high-salinity mineralized mine water from Ningdong to improve the utilization rate of mine wastewater; (2) characterize the damage and fouling of the membrane during long-term MD; and (3) explore the connection between fouling and permeate quality.

2 Materials and methods

2.1 Characteristics of pretreated mine water

The mine water sample was colorless and transparent with no suspended solids. The Cl^- and SO_4^{2-} contents of the mine water after hardening pretreatment with caustic soda are shown in Table 1. Hardening pretreatment reduced the hardness of the water from 1352.71 to 183.87 mg/L. The contents of organic matter and petroleum were also reduced, thereby reducing the risk of organic fouling on the membrane.

2.2 Membrane material used in VMD

Table 2 lists the main characteristics of the polyvinylidene fluoride (PVDF) hollow-fiber membrane used in the experiment. The hollow fibers were gathered in a plastic tube to form a membrane module. As shown in Fig. 2a, the membrane pores presented an irregular, tear-like pore structure with a large number of microfibers distributed among the pores. The overall cross section (Fig. 2b) had an

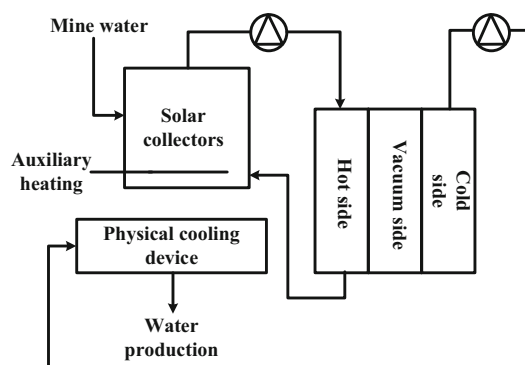


Fig. 1 Diagram of a solar photothermal VMD system

Table 1 Cl^- and SO_4^{2-} contents of pretreated mine water

Component	Concentration
Cl^- (g/L)	1888.75
SO_4^{2-} (mg/L)	1880.23
K^+ (mg/L)	13.92
Na^+ (mg/L)	1954.66
Conductivity (ms/cm)	10.32
Mineralization	6380
COD_{Cr} (mg/L)	21
pH	10.25

Table 2 Key characteristics of the PVDF hollow-fiber membrane module

Parameter	Measured result
Outer diameter (mm)	1.139
Inner diameter (mm)	0.849
Average pore size (μm)	0.16
Porosity (%)	85
Contact angle (°)	106.5
Effective membrane surface area (m ²)	0.1066

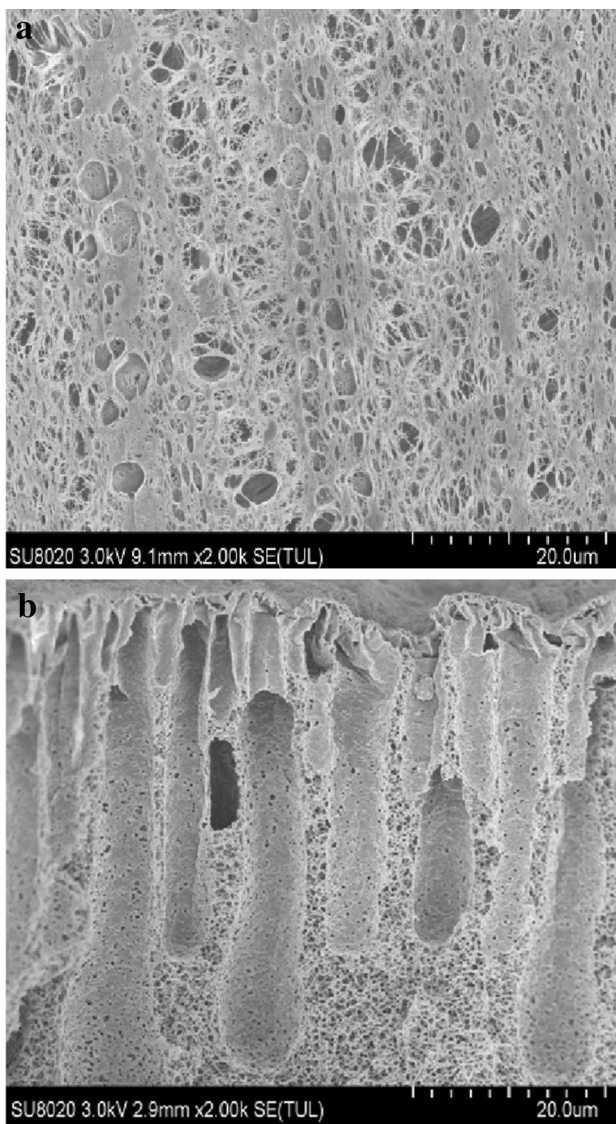


Fig. 2 SEM micrographs of the PVDF hollow-fiber membrane: **a** inner membrane surface and **b** cross section

asymmetric shape with irregular, finger-like microporous structures underneath the skin layer.

2.3 Experimental methods

2.3.1 Response surface optimization (RSM)

Numerous factors can affect the stable operation of VMD. Therefore, RSM based on a Box-Behnken design was employed to statistically analyze the VMD parameters. In the present work, the feed temperature (60–75 °C), flow rate (1–2.5 L/min), and vacuum pressure (– 0.045 to 0.09 MPa) were investigated with the permeate flux as the response variable.

2.3.2 Continuous VMD operation

The lab-scale VMD system used in the experiment is shown in Fig. 3. The system primarily includes the hot side, cold side loop, and PVDF hollow-fiber membrane module. The parameters for VMD operation were set according to the RSM results.

Before the test, the feed solution was poured into the liquid tank through the water injection hole. The outlet of the membrane module was connected to the condenser to ensure that the cooling temperature met the requirements. The feed solution was then heated to the set temperature using a heating element, and the solution was continuously pumped into the membrane module by the peristaltic pump. The feed flow rate was adjusted to a preset value by the liquid flow meter. When the inlet and outlet temperatures of the membrane module became stable, the vacuum pump was turned on to provide the vacuum pressure required for the experiment. The water quantity could be observed through the electronic balance connected to the water collector. The produced water was sampled and tested every hour, and the changes in conductivity and pH were recorded over time.

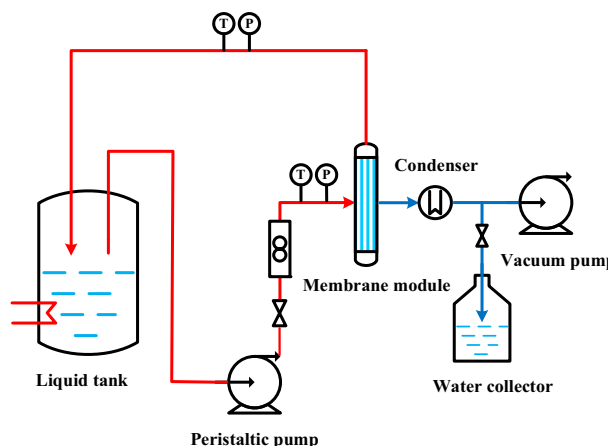


Fig. 3 Schematic of the experimental VMD system

When the conductivity of the produced water increased significantly, the membrane module was cleaned in two steps. First, the VMD device was cleaned with tap water for 30 min (1.50 L/min). Second, the membrane module was dried in an oven at 50 °C for 30 min.

The membrane flux J (kg/(m² h)) was calculated as

$$J = \frac{N}{A \times t} \quad (1)$$

where, N is the mass of permeate water (kg); A is the membrane area (m²); and t is the operation time (h).

The salt rejection rate R (%) was determined as

$$R = \left(\frac{\delta_0 - \delta_t}{\delta_0} \right) \times 100\% \quad (2)$$

where, δ_0 is the initial conductivity (μS/cm) of the feed solution, and δ_t is the conductivity (μS/cm) of the permeate water at time t .

2.4 Analytical measurements

After the experiment, the contaminated membrane was sampled and compared with the original membrane. The surface and cross-sectional morphologies of the membrane were examined by scanning electron microscopy (SEM; Hitachi SU8020). The SEM samples were prepared by immersing the membrane in liquid nitrogen. Energy-dispersive X-ray spectroscopy (EDS) was used to determine the elemental composition of the membrane.

The membrane contact angle was determined using a goniometer (ramé-hart Model 250) at room temperature. The membrane was cut longitudinally and fixed on the test bench. For each sample, the measurement was repeated five times at different spots, and the measurement results were averaged.

The conductivity and pH of the feed and distillate were monitored using a conductivity meter (Lightning DZS-708A). The ionic contents of the feed and distillate were measured using an ion chromatograph (Epoch EP-600).

3 Results and discussion

3.1 Effects of multiple factors on MD performance

As shown in Table 3, the F value of the model term developed by the ANOVA was 29.79, and the P value was less than 0.0001, indicating that the regression equation had high significance (Devi et al. 2019). Generally, a larger F value and a smaller P value correspond to a more significant correlation (Jamekhorshid et al. 2014). The

Table 3 ANOVA results of the RSM

Source	Sum of squares	D_f	Mean square	F value	P value	Distinctiveness
Model	50.39	9	5.60	29.79	< 0.0001	**
A (vacuum pressure)	37.35	1	37.35	198.70	< 0.0001	**
B (temperature)	6.96	1	6.96	37.04	0.0005	
C (flow rate)	0.16	1	0.16	0.84	0.3899	
AB	1.44	1	1.44	7.65	0.0278	*
A ²	4.14	1	4.14	22.05	0.0022	**
Residual	1.32	7	0.19			
Lack of fit	0.62	3	0.21	1.17	0.4244	
Pure error	0.70	4	0.17			
Cor total	51.71	16				

*Indicates that the effect of the result is significant ($P < 0.05$), ** indicates that the result is extremely significant ($P < 0.01$)

quadratic model for RSM in terms of the evaluated factors is represented as Eq. (3):

$$y_{\text{flux}} = 33.59 + 408.85A - 0.667B - 4.386C - 3.554AB + 0.369AC + 0.077BC + 1959.61A + 3.37387B - 0.03B^2 - 0.1107C^2. \quad (3)$$

which A refers to the vacuum pressure, B refers to the feed temperature, C refers to the flow rate, According to the analysis of variance (ANOVA), the primary and secondary order of the influence of three factors on cleaning efficiency was: vacuum pressure (A) > temperature (B) > flow rate (C). A and B also had significant influences on each other. According to the experimental results, the optimal VMD parameters were a vacuum pressure of −0.09 MPa, a temperature of 70 °C, and a flow rate of 1.50 L/min.

As shown in Fig. 4, among the evaluated parameters, vacuum pressure had the greatest effect on the VMD process. Vacuum pressure was linearly related to water production. Similarly, Xing et al. (2017) found that the flow of permeable fluid increased linearly when the vacuum pressure was reduced from 0.6 to 0.98 atm. These findings can be attributed to the fact that the transmembrane pressure difference is proportional to the steam driving force on both sides of the membrane module during the VMD process. The critical vacuum pressure in this experiment was calculated to be 0.0614 MPa. Pengyuan et al. (2019) reached similar conclusions when using MD to treat high-salinity wastewater.

The second most influential parameter on VMD was feed temperature. The membrane flux increased with increasing temperature. According to the empirical formula of Antoine (Morillon et al. 1999), the vapor pressure

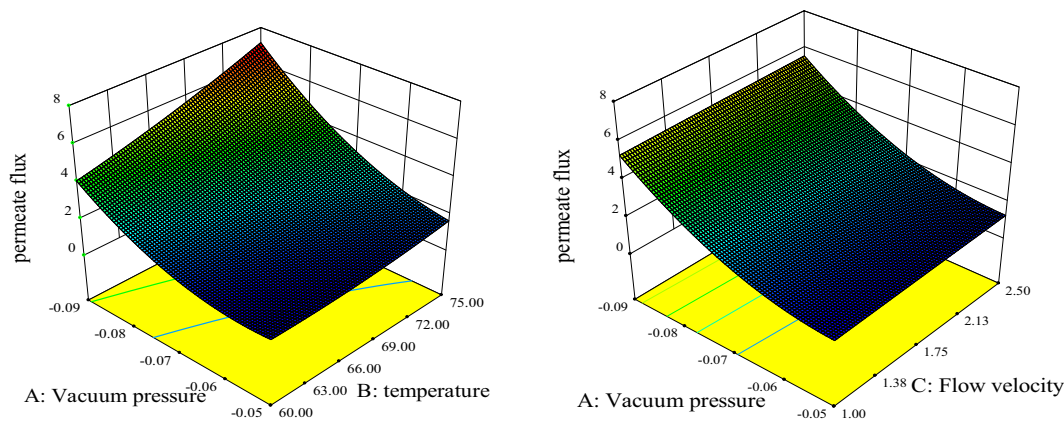


Fig. 4 Contour and response surface plots showing the effects of vacuum pressure (MPa), feed temperature (°C), and feed flow rate (L/min) on permeate flux (kg/(m² h))

depends on the temperature, and increasing the feed temperature can increase the vapor pressure:

$$N = \frac{1}{\frac{1}{CK} + \frac{1}{CM}} \times (P_f - P_d) \tag{4}$$

where, *N* is the flux; *P_f* and *P_d* are the water vapor pressures at the feed liquid/membrane and membrane/distillate interfaces, respectively; and *CK* and *CM* are the mass transfer coefficients of Knudsen diffusion and molecular diffusion, respectively.

Among the three evaluated factors, the feed flow rate had the weakest influence on VMD. As the feed flow rate increased in the beginning of the VMD process, the effects of concentration and temperature polarization were significantly reduced, resulting in an increase in permeate flux. Subsequently, the permeate flux stabilized as the flow rate continued to increase, and the feed flow changed from laminar flow to turbulent flow, and the thickness of temperature interface layer and ion interface layer decrease with the change of flow pattern. As the flow rate increased further, the thickness of the temperature boundary layer and the ion interface layer would not continue to weaken. Thereby, increasing the flow rate did not further enhance the permeate flux (Pengyuan et al. 2019).

3.2 Continuous VMD operation

VMD was operated continuously using the optimal process parameters. As shown in Fig. 5, at the beginning of the experiment, the flux was stable at 11.2 kg/(m² h), the conductivity of produced water was 8.5 μS/cm, and the salt rejection rate reached 99.9%. After 26 h of operation, the flux began to decrease gradually and became stable at 8.22 kg/(m² h), and the salt rejection rate decreased to 95.5%. After 41 h of constant operation, the water quality deteriorated rapidly. For instance, the conductivity

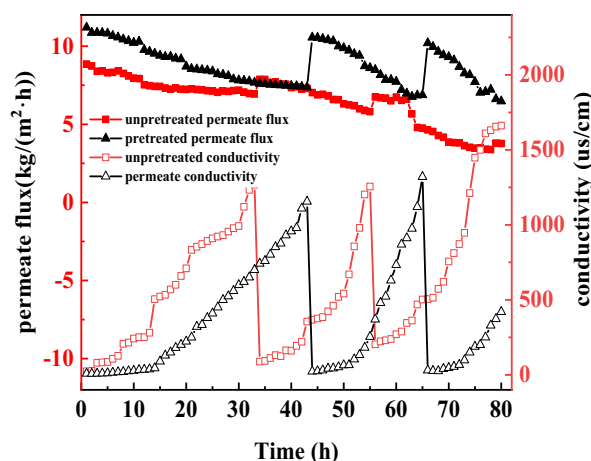


Fig. 5 Permeate flux and produced water conductivity vs. time during the VMD treatment of pretreated and untreated mine water

increased to 980 μS/cm, the flux decreased to 7.45 kg/(m² h), and the salt rejection rate was only 90.2%. Based on these experimental results, the membrane module was cleaned. After the first cleaning, the flux recovered to 10.56 kg/(m² h), and the salt rejection rate recovered to 99.77%. At 61 h, the flux decreased from 10.56 to 7.73 kg/(m² h), and the salt rejection rate dropped to 91.3%. At 66 h, the membrane was cleaned twice using the above cleaning method. After the second cleaning, the flux decreased rapidly to 75% of its initial value within 9 h and then decreased further to approximately 6.48 kg/(m² h) within 5 h.

According to the changes in flux and water quality over time, the VMD process could be divided into the following three stages. The initial stage of rapid flux decline can be regarded as the membrane wetting stage. Due to concentration polarization, inorganic salt ions were adsorbed and deposited on the membrane surface, leading to the wetting of membrane pores along with reductions in membrane

effective area and flux. As shown in Fig. 4, the flux was only reduced by 21.6%, indicating that the number of wetted membrane pores was small. However, the solute passed through the membrane from the feed side to the permeate side, and the conductivity of the produced water increased greatly. The second stage (after the first cleaning) was characterized by moderate membrane fouling and a large decrease in flux because inorganic salt ions gradually reached saturation and crystallized on the membrane surface, and membrane fouling replaced membrane wetting. Finally, the third stage was characterized by a rapid decline in flux in a short time period and can be regarded as the stage of fouling layer formation. As the continuous VMD run time increased, numerous inorganic salt ions accumulated and compacted, forming a fouling layer that covered the surface of the membrane. The presence of this layer prevented water vapor from passing through the membrane (Guillen-Burrieza et al. 2014).

The trends in flux and conductivity over time were similar for pretreated and untreated mine water. However, due to its higher content of inorganic salts (e.g., calcium and magnesium salts) and higher hardness, the flux decline of the untreated mine water was relatively large (Fig. 5). Thus, pretreatment slowed the increase in membrane pressure difference and membrane fouling to some extent, although it could not prevent irreversible membrane fouling. Thus, the development of inorganic fouling should be further evaluated.

Only physical cleaning was used in this study for the following reasons. First, physical cleaning is fast and involves simple steps. The waste liquid produced by the cleaning process produces minimal environmental pollution and does not result in membrane corrosion. In addition, the cost of cleaning and replacing membrane components accounts for 70% of the total cost of the membrane separation process (Geata et al. 1995), and physical cleaning can result in significant cost savings. Targeted cleaning methods and cleaning agents can be reasonably selected based on the physical and chemical properties of the membrane pollutants and the cleaning requirements.

Compared to the mine water, the quality of the produced water was greatly improved. The conductivity of the permeate water was 23.9 $\mu\text{S}/\text{cm}$, the salt rejection rate reached 99.1%, and the content of total dissolved solids was 11.32 mg/L. According to the national standards (GB8978–1996 and GB5084–92), the produced water in this study can be reused to irrigate farmland or in nearby industries such as power plants to reduce water costs (Julian et al. 2018).

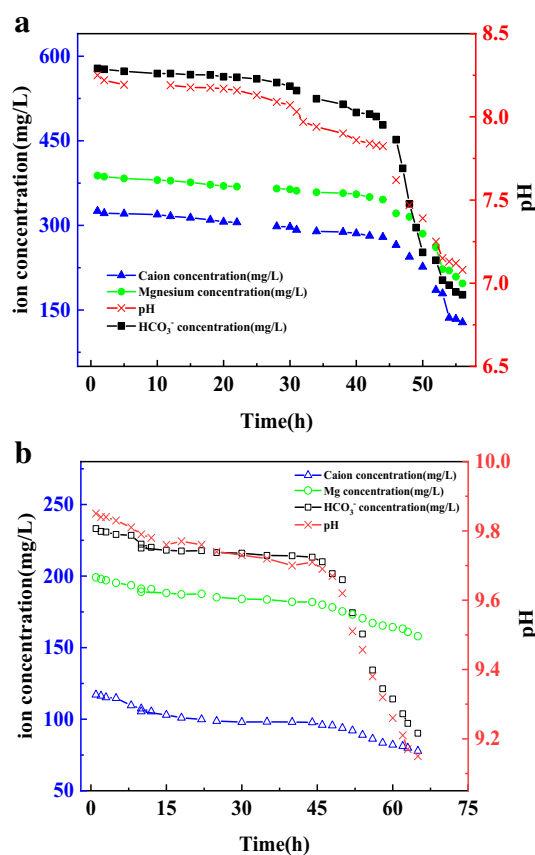


Fig. 6 Solution Ca^{2+} , HCO_3^- , and Mg^{2+} concentrations and pH vs. time for **a** untreated mine water and **b** pretreated mine water under the optimal experimental conditions (temperature = 70 °C, pressure = - 0.09 MPa, and flow rate = 1.5 L/min)

3.3 Scaling behavior

Previous studies have revealed that CaCO_3 precipitation is related to the change in pH of the feed during MD operation (He et al. 2009). As shown in Fig. 6a, the pH of the untreated mine water decreased from 8.25 to 7.94 before the first cleaning. The change in pH was almost consistent with the observed change in flux (Fig. 5a). During the first 31 h of continuous operation, the decomposition of HCO_3^- was the main process due to the high concentration of HCO_3^- . Moreover, HCO_3^- was decomposed to produce CO_2 , most of which was dissolved in the feed solution, resulting in a gradual decrease in pH. After 34 h of continuous VMD, the membrane module was cleaned. The scale remaining on the membrane after cleaning may have provided a location for crystallization, resulting in faster crystallization (Martinetti et al. 2009). Therefore, between 45 and 54 h, the contents of HCO_3^- and Ca^{2+} declined significantly due to the precipitation of CaCO_3 from supersaturated solution. The content of Mg^{2+} in the feed solution also decreased during this period, indicating that the CaCO_3 precipitates incorporated Mg^{2+} .

In addition, CaCO_3 precipitation and the decomposition of HCO_3^- occurred almost simultaneously, generating a large amount of CO_2 . This CO_2 reacted with the solution to generate H_2CO_3 , eventually leading to a significant decrease in pH. After 56 h of continuous VMD operation, the pH increased slightly because the generation of CO_2 slowed down. During the VMD process, Ca^{2+} decreased by 197.64 mg/L, Mg^{2+} decreased by 191.21 mg/L, and HCO_3^- decreased by 401.25 mg/L, demonstrating that some Ca^{2+} did not combine with HCO_3^- and may have formed CaSO_4 . The presence of a small amount of CaSO_4 scaling was confirmed by EDS elemental analysis.

As shown in Fig. 6b, the gradual declines in Ca^{2+} , Mg^{2+} , and HCO_3^- concentrations during VMD operation were similar for the pretreated mine water as for the untreated water (Fig. 6a). Due to the addition of CaO and Na_2CO_3 during the pretreatment process, the initial pH of the feed solution was 9.85, and the pH became stable at 9.15. The HCO_3^- content decreased from 233.15 to 80.2 mg/L during VMD. Therefore, the pretreatment process effectively alleviated the crystallization of calcium-related soluble salts. Zhang et al. (2015) explored seawater reverse osmosis brine during direct contact MD operation and found that the change in conductivity may be related to the accumulation of CO_2 in the feed solution. CO_2 was then transported through the membrane, and HCO_3^- was produced on the permeate side, increasing the conductivity.

3.4 Membrane fouling analysis

To further determine the composition of pollutants on the membrane surface, the membrane fouling layer was analyzed. After the experiment, the membrane module was disconnected. The feed inlet was covered by a large amount of yellowish-brown sediment, and the membrane fibers had become fragile. As shown in Fig. 7c, due to the direct contact between the inner membrane surface and the mine water, the inner membrane was seriously polluted, and the membrane pores were almost completely covered by crystals and fouling layers. Since the composition of the mine water was not complex, the composition of the fouling layer was relatively simple. Two primary crystal forms (needle-like and spherical) were observed on the inner membrane surface, and the main crystalline component was CaCO_3 . The shape and size of the crystals agreed with those reported by Naidu et al. (2017). This suggests that the content of organic matter in the mine water was low because the presence of organic matter would decompose these CaCO_3 crystals into small rhombohedral colloids.

The content of Na on the outer membrane surface was higher than that on the inner surface, and its weight percentage exceeded 6% (Table 4). Meanwhile, the contents

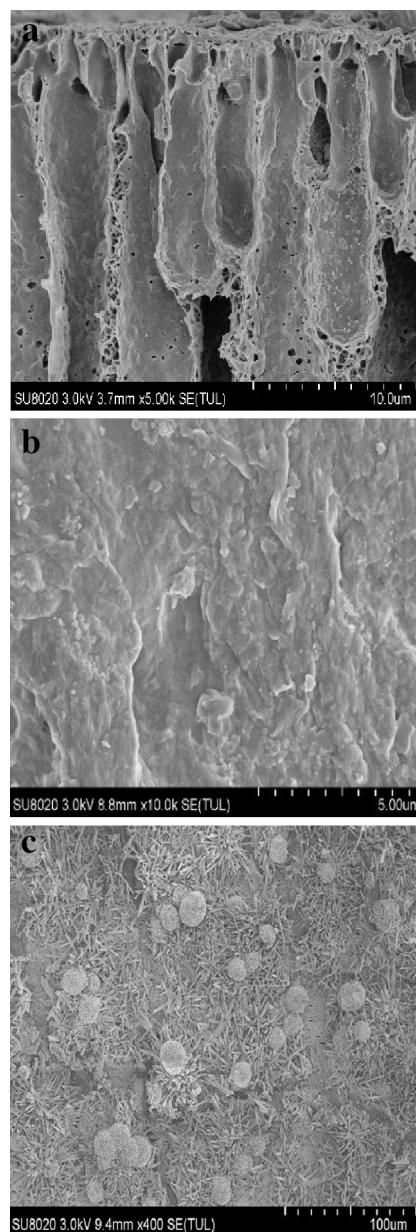


Fig. 7 SEM images of a fouled PVDF hollow-fiber membrane: **a** cross section, **b** outer surface, and **c** inner surface

of Ca and Mg were very low. Combined with the experimental results in Sect. 2.2, these findings confirm that membrane wetting occurred during VMD operation. Further, the evaporation of the feed and frequent temperature changes can lead to supersaturated conditions, resulting in the nucleation of NaCl crystals on the outer surface of the membrane (Pengfei et al. 2017). The membrane wetting observed in this study could be attributed to two main factors. First, inorganic salts were adsorbed on the membrane surface, altering the surface energy of the membrane and eventually triggering membrane wetting (Geata et al. 1995). After fouling, the membrane contact angle

Table 4 Elemental compositions of the PVDF hollow-fiber membrane before and after fouling based on EDS analysis

Element	Weight percentage (%)			
	Inner membrane before fouling	Inner membrane after fouling	Outer membrane after fouling	Membrane cross section after fouling
C	46.47	37.55	37.36	35.81
O	3.64	18.14	9.10	12.48
F	49.34	5.72	32.03	41.61
Na	0.00	1.58	6.71	4.24
Mg	0.00	5.86	0.32	1.18
S	0.55	0.65	1.65	1.12
Cl	0.00	0.95	7.81	2.86
Ca	0.00	28.55	0.00	0.70

decreased to 32.1°, indicating that fouling changed the properties of the membrane itself. Second, during water evaporation, the NaCl crystals on the membrane surface moved, resulting in the slight tearing of the membrane and promoting salt deposition and subsequent wetting (Meng et al. 2014). At the same time, the cross section of the membrane was partially covered by the sediment layer (Fig. 7a), and EDS analysis indicated a similar elemental composition to the layer on the outer surface of the membrane. Due to membrane wetting, these contaminants can penetrate deep into the membrane pores, causing fouling in the membrane pores. The above analysis clearly shows that the main source of contamination in the VMD treatment of mine water is calcium precipitation. The occurrence of precipitation leads to decreased flux and membrane pore wetting. Future studies should focus on improving this problem from two aspects: (1) after the mine water is hardened, the nanofiltration device can be added to further improve the feed water quality; and (2) acid cleaning can be included as a component of membrane cleaning to remove calcium pollutants, thereby extending the membrane service life and MD run time.

4 Conclusions

(1) Increasing the temperature, flow rate, and vacuum pressure within a reasonable range all resulted in increased flux, with the influence of vacuum pressure being the most significant. Without considering energy consumption and economy, the optimal operating parameters were determined as temperature = 70 °C, feed flow rate = 1.5 L/min, and pressure = -0.09 MPa. Under these conditions, the

membrane flux reached 8.85 kg/(m² h), and the salt rejection rate was 99.7%.

- (2) During VMD operation, the flux and desalination rate of the mine water decreased to 55% and 72% of their initial values, respectively. The fouling process could be divided into three stages: membrane wetting, crystallization, and fouling layer formation. The rapid development of crystallization-based fouling was attributed to changes in the pH and bicarbonate content of the mine water, and the pH was an important factor in the rapid decline of permeability in the early fouling stage.
- (3) During the continuous operation of VMD, the inner surface of the membrane was seriously fouled, and most of the membrane pores were covered by crystalline precipitates and sediment layers. According to EDS elemental analysis, the fouling was mainly caused by calcium ions in the mine water. SEM analysis showed that the crystal diameter was much larger than the membrane pore size; thus, no calcium crystals were observed on the cross section or outer surface of the membrane. The main contaminant found on the cross section and outer surface of the membrane was NaCl. NaCl contamination was caused by membrane wetting and the penetration of the mine water into the membrane pores at the beginning of VMD operation.

Acknowledgements This research was supported by the Open Fund Project of the State Key Laboratory of Water Resources Protection and Utilization in Coal Mining (GJNY-18-73.13).

Open Access This article is licensed under a Creative Commons Attribution 4.0 International License, which permits use, sharing, adaptation, distribution and reproduction in any medium or format, as long as you give appropriate credit to the original author(s) and the source, provide a link to the Creative Commons licence, and indicate if changes were made. The images or other third party material in this article are included in the article's Creative Commons licence, unless indicated otherwise in a credit line to the material. If material is not included in the article's Creative Commons licence and your intended use is not permitted by statutory regulation or exceeds the permitted use, you will need to obtain permission directly from the copyright holder. To view a copy of this licence, visit <http://creativecommons.org/licenses/by/4.0/>.

References

- Alkudhiri A, Darwish N, Hilal N (2012) Membrane distillation: a comprehensive review. *Desalination* 287:2–18. <https://doi.org/10.1016/j.desal.2011.08.027>
- Dazhao Gu, Yong Z, Zhiguo C (2016) Technical progress of water resource protection and utilization by coal mining in China. *Coal Sci Technol* 44:1–7
- Devi KRS, Mathew S, Rajan R et al (2019) Biogenic synthesis of g-C₃N₄/Bi₂O₃ heterojunction with enhanced photocatalytic

- activity and statistical optimization of reaction parameters. *Appl Surf Sci* 494:465–476. <https://doi.org/10.1016/j.apsusc.2019.07.125>
- Drioli E, Ali A, Macedonio F (2015) Membrane distillation: recent developments and perspectives. *Desalination* 356:56–84. <https://doi.org/10.1016/j.desal.2014.10.028>
- Fuqin Li, Guifeng Z, Yunhao Z et al (2018) Research on Zero Drainage Process of Highly Mineralized Mine Water. *Coal Sci Technol* 46:81–86
- Geata SN (1995) In *Membrane technology: Application to industrial wastewater treatment*. Kluwer Academic Publishers, Dordrecht
- Guillen-Burrieza E, Ruiz-Aguirre A (2014) Membrane fouling and cleaning in long term plant-scale membrane distillation operations. 2014. *J Membr Sci* 468:360–372. <https://doi.org/10.1016/j.memsci.2014.05.064>
- Guillen-Burrieza E, Thomas R, Mansoor B et al (2013) Effect of dry-out on the fouling of PVDF and PTFE membranes under conditions simulating intermittent seawater membrane distillation (SWMD). *J Membr Sci* 438:126–139. <https://doi.org/10.1016/j.memsci.2013.03.014>
- He F, Sirkar KK, Gilron J (2009) Effects of antiscalants to mitigate membrane scaling by direct contact membrane distillation. *J Membr Sci* 345:53–58. <https://doi.org/10.1016/j.memsci.2009.08.021>
- Jamekhorshid A, Sadrameli SM, Bahramian AR (2014) Process optimization and modeling of microencapsulated phase change material using response surface methodology. *Appl Therm Eng* 70:183–189
- Jiang Binbin Hu, Xiaolong GQ et al (2018) Research on underground classification treatment technology of highly mineralized mine water in Lingxin Coal Mine. *Coal Eng* 50:83–85
- Julian H, Lian B, Li H et al (2018) Numerical study of CaCO₃ scaling in submerged vacuum membrane distillation and crystallization (VMDC). *J Membr Sci* 559:87–97. <https://doi.org/10.7836/kses.2014.34.5.023>
- Laqbaqbi M, García-Payo MC, Khayet M et al (2018) Application of direct contact membrane distillation for textile wastewater treatment and fouling study. *Sep Purif Technol* 209:815–825. <https://doi.org/10.1016/j.seppur.2018.09.031>
- Limin F, Ma Liqiang Yu, Yihe WS, Yujun Xu (2019) Water-conserving mining influencing factors identification and weight determination in northwest China. *Int J Coal Sci Technol* 6(1):95–101. <https://doi.org/10.1007/s40789-018-0233-2>
- Martinetti CR, Childress AE, Cath TY (2009) High recovery of concentrated RO brines using forward osmosis and membrane distillation. *J Membr Sci* 331:31–39. <https://doi.org/10.1016/j.memsci.2009.01.003>
- Meng S, Ye Y, Mansouri J et al (2014) Fouling and crystallization behavior of superhydrophobic nano-composite PVDF membranes in direct contact membrane distillation. *J Membr Sci* 463:102–111. <https://doi.org/10.1016/j.memsci.2014.03.027>
- Ministry of Water Resources of the People's Republic of China (2018) *China Water Resources Bulletin*
- Morillon V, Debeaufort F, Jose J et al (1999) Water vapour pressure above saturated salt solutions at low temperatures. *Fluid Phase Equilib* 155(2):297–309
- Naidu G, Jeong S (2017) Membrane distillation for wastewater reverse osmosis concentrate treatment with water reuse potential. *J Membr Sci* 524:565–575
- Pengfei R, Yongqiang Y, Xinmiao Z (2017) Research progress on the formation and prevention of pollution during membrane distillation. *Modern Chemical Industry* 05:48–51
- Pengyuan D, Wei D (2019) Experimental study on the treatment of simulated high-salt wastewater by vacuum membrane distillation technology. *Sci Technol Eng* 19:275–280
- Sun AC, Kosar W, Zhang Y et al (2014) Vacuum membrane distillation for desalination of water using hollow fiber membranes. *J Membr Sci* 455:131–142. <https://doi.org/10.1016/j.memsci.2013.12.055>
- Wang NQ (1999) *Principles of chemical engineering*. Chengdu University of Science and Technology Press, China
- Bian Wei, Li Jingfeng, Gu Dazhao et al (2020) Water film distillation treatment technology for high salinity mines in western mining area [J/OL]. *Coal Sci Technol* 1–7(2020–03–05).
- Xing Y, Qi C, Feng H et al (2017) Performance study of a pilot-scale multi-effect vacuum membrane distillation desalination plant. *Desalination* 403:199–207. <https://doi.org/10.1016/j.desal.2016.07.008>
- Zhang P, Knötig P, Gray S et al (2015a) Scale reduction and cleaning techniques during direct contact membrane distillation of seawater reverse osmosis brine. *Desalination* 374:20–30. <https://doi.org/10.1016/j.desal.2015.07.005>. Alkudhiri A, Darwish N, Hilal N (2012) Membrane distillation: a comprehensive review. *Desalination* 287:2–18. <https://doi.org/10.1016/j.desal.2011.08.027>